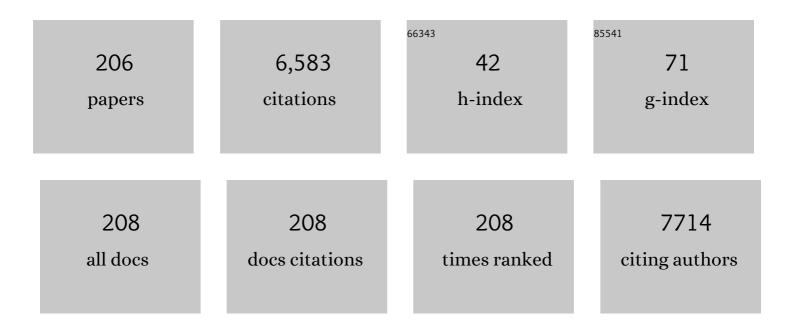
List of Publications by Year in descending order

Source: https://exaly.com/author-pdf/5831522/publications.pdf Version: 2024-02-01



YUNRIN HE

#	Article	IF	CITATIONS
1	Ultrasensitive selfâ€powered UV PDs via depolarization and heterojunction fields jointly enhanced carriers separation. Journal of the American Ceramic Society, 2022, 105, 392-401.	3.8	8
2	Nb-doped VO2 thin films with enhanced thermal sensing performance for uncooled infrared detection. Materials Research Bulletin, 2022, 146, 111615.	5.2	16
3	Evaporation crystallization of zero-dimensional guanidinium bismuth iodide perovskite single crystal for X-ray detection. Inorganic Chemistry Frontiers, 2022, 9, 494-500.	6.0	11
4	Au-PEDOT/rGO nanocomposites functionalized graphene electrochemical transistor for ultra-sensitive detection of acetaminophen in human urine. Analytica Chimica Acta, 2022, 1191, 339306.	5.4	13
5	Solutionâ€gated transistor based on electrochemically reduced graphene oxide channel. Journal of Materials Science, 2022, 57, 4652-4663.	3.7	1
6	Multi-component ZnO alloys: Bandgap engineering, hetero-structures, and optoelectronic devices. Materials Science and Engineering Reports, 2022, 147, 100661.	31.8	58
7	The elastic, electron, phonon, and vibrational properties of monolayer XO2 (XÂ=ÂCr, Mo, W) from first principles calculations. Materials Today Communications, 2022, 30, 103183.	1.9	6
8	Flexible fast responding solar-blind photodetectors based on (TmGa)2O3 films grown on mica. Applied Physics Letters, 2022, 120, .	3.3	9
9	High-performance Pt/Ti3C2Tx MXene based graphene electrochemical transistor for selective detection of dopamine. Analytica Chimica Acta, 2022, 1201, 339653.	5.4	28
10	Ca Solubility in a BiFeO ₃ -Based System with a Secondary Bi ₂ O ₃ Phase on a Nanoscale. Journal of Physical Chemistry C, 2022, 126, 7696-7703.	3.1	1
11	Polymer composites with high energy density and charge–discharge efficiency at high temperature using aluminum oxide particles. Journal of Materials Research and Technology, 2022, 18, 4367-4374.	5.8	11
12	Energy density and efficiency of scalable polymer nanocomposites utilizing core-shell PLZST@Al2O3 antiferroelectric fillers with dielectric gradient. Chemical Engineering Journal, 2022, 446, 136925.	12.7	15
13	Ag nanocubes monolayer-modified PDMS as flexible SERS substrates for pesticides sensing. Mikrochimica Acta, 2022, 189, .	5.0	17
14	High-performance self-driven ultraviolet photodetector based on SnO2 p-n homojunction. Optical Materials, 2022, 129, 112571.	3.6	6
15	Monolayer SnX (X = O, S, Se): Two-Dimensional Materials with Low Lattice Thermal Conductivities and High Thermoelectric Figures of Merit. ACS Applied Energy Materials, 2022, 5, 7802-7812.	5.1	20
16	XTIO (XÂ=ÂK, Rb, Cs): Novel 2D semiconductors with high electron mobilities, ultra-low lattice thermal conductivities and high thermoelectric figures of merit at room temperature. Applied Surface Science, 2022, 599, 153924.	6.1	20
17	BeCaZnO quaternary alloy: thin films and ultraviolet photodetectors. Journal of Alloys and Compounds, 2021, 857, 157567.	5.5	6
18	Excellent energy storage properties over a wide temperature range under low driving electric fields in NBT-BSN lead-free relaxor ferroelectric ceramics. Ceramics International, 2021, 47, 4715-4721.	4.8	26

#	Article	IF	CITATIONS
19	Novel graphene electrochemical transistor with ZrO2/rGO nanocomposites functionalized gate electrode for ultrasensitive recognition of methyl parathion. Sensors and Actuators B: Chemical, 2021, 328, 128936.	7.8	34
20	The influence of Cd-alloying on the light-emission properties of 2D butylammonium lead chloride perovskite. Materials Letters, 2021, 282, 128847.	2.6	1
21	Carbon encapsulation of MoS2 nanosheets to tune their interfacial polarization and dielectric properties for electromagnetic absorption applications. Journal of Materials Chemistry C, 2021, 9, 537-546.	5.5	13
22	Diamine tailored smooth and continuous perovskite single crystal with enhanced photoconductivity. Journal of Materials Chemistry C, 2021, 9, 1303-1309.	5.5	14
23	Depolarization electric field and poling voltageâ€modulated Pb,La(Zr,Ti)O ₃ â€based selfâ€powered ultraviolet photodetectors. Journal of the American Ceramic Society, 2021, 104, 928-935.	3.8	21
24	Achieving p-type conductivity in wide-bandgap SnO2 by a two-step process. Applied Physics Letters, 2021, 118, .	3.3	12
25	Modification with platinum of silver-deposited nickel wire electrodes for electrocatalytic oxidation of alcohols. Electrochemistry Communications, 2021, 124, 106939.	4.7	5
26	Formation of a Stable Guanidinium–Formamidinium Phase in Bismuth Chloride Perovskites with Broadband Emission. Chemistry of Materials, 2021, 33, 3258-3265.	6.7	14
27	Interface control of tetragonal ferroelectric phase in ultrathin Si-doped HfO2 epitaxial films. Acta Materialia, 2021, 207, 116696.	7.9	17
28	Enhancing visible-light transmittance while reducing phase transition temperature of VO2 by Hf–W co-doping. Applied Physics Letters, 2021, 118, .	3.3	21
29	Conjugated Ditertiary Ammonium Templated (100)-Oriented 2D Perovskite with Efficient Broad-Band Emission. Chemistry of Materials, 2021, 33, 4456-4464.	6.7	23
30	Nb-doped ZrxSn1â^'xO2: Experimental and first-principles study. Journal of Applied Physics, 2021, 130, .	2.5	2
31	Codeposition of Platinum and Gold on Nickel Wire Electrodes via Galvanic Replacement Reactions for Electrocatalytic Oxidation of Alcohols. ACS Omega, 2021, 6, 18395-18403.	3.5	10
32	A novel electrochemical sensor via Zr-based metal organic framework–graphene for pesticide detection. Journal of Materials Science, 2021, 56, 19060-19074.	3.7	30
33	Intermolecular Hydrogen-Bonding Correlated Structure Distortion and Broadband White-Light Emission in 5-Ammonium Valeric Acid Templated Lead Chloride Perovskites. Crystal Growth and Design, 2021, 21, 5731-5739.	3.0	13
34	An effective strategy to realize superior high-temperature energy storage properties in Na0.5Bi0.5TiO3 based lead-free ceramics. Ceramics International, 2021, 47, 25794-25799.	4.8	6
35	Correlating point defects with mechanical properties in nanocrystalline TiN thin films. Materials and Design, 2021, 207, 109844.	7.0	18
36	Highâ€Performance Selfâ€Powered Ultraviolet Photodetector based on Coupled Ferroelectric Depolarization Field and Heterojunction Builtâ€In Potential. Advanced Electronic Materials, 2021, 7, 2100717.	5.1	26

#	Article	IF	CITATIONS
37	Controllable preparation of (200) facets preferential oriented silver nanowires for non-invasive detection of glucose in human sweat. Smart Materials in Medicine, 2021, 2, 150-157.	6.7	6
38	The formation of TiO ₂ /VO ₂ multilayer structure <i>via</i> directional cationic diffusion. Nanoscale, 2021, 13, 7783-7791.	5.6	10
39	Antisolventâ€assisted Crystallization of Centimeterâ€sized Leadâ€free Bismuth Bromide Hybrid Perovskite Single Crystals with Xâ€ray Sensitive Merits. Chemistry - an Asian Journal, 2021, 16, 4137-4144.	3.3	10
40	Tunable bandgap and luminescence characters in single-phase two-dimensional perovskite AVA2PbCl Br4- alloys. Journal of Materials Research and Technology, 2021, 15, 5353-5359.	5.8	3
41	The S-content-dependent lattice structure evolution and bandgap modulation in quaternary MgZnOS alloy films. Journal Physics D: Applied Physics, 2021, 54, 065104.	2.8	1
42	Effects of the film thickness and poling electric field on photovoltaic performances of (Pb,La)(Zr,Ti)O3 ferroelectric thin film-based devices. Ceramics International, 2020, 46, 4148-4153.	4.8	28
43	Non-invasive detection of glucose <i>via</i> a solution-gated graphene transistor. Analyst, The, 2020, 145, 887-896.	3.5	27
44	Combined Fe and O effects on microstructural evolution and strengthening in Cu–Fe nanocrystalline alloys. Materials Science & Engineering A: Structural Materials: Properties, Microstructure and Processing, 2020, 772, 138800.	5.6	16
45	High-temperature energy storage properties in polyimide-based nanocomposites filled with antiferroelectric nanoparticles. Journal of Materials Research and Technology, 2020, 9, 11344-11350.	5.8	16
46	Codeposition of Palladium and Gold on Nickel Wire Electrodes via Galvanic Replacement Reactions for Ethanol Oxidation. ACS Applied Energy Materials, 2020, 3, 7083-7090.	5.1	3
47	Enhanced photovoltaic effect in Ca and Mn co-doped BiFeO3 epitaxial thin films. Applied Surface Science, 2020, 530, 147194.	6.1	50
48	Highly Sensitive and Tunable Self-Powered UV Photodetectors Driven Jointly by p-n Junction and Ferroelectric Polarization. ACS Applied Materials & Interfaces, 2020, 12, 53957-53965.	8.0	65
49	PLD growth and characteristics of lead-free NKLNST ferroelectric nanotubes. Journal of Materials Research and Technology, 2020, 9, 12818-12823.	5.8	1
50	Improving electrical properties and toughening of PZT-based piezoelectric ceramics for high-power applications via doping rare-earth oxides. Journal of Materials Research and Technology, 2020, 9, 14254-14266.	5.8	18
51	High-temperature energy storage performances in (1-x)(Na0.50Bi0.50TiO3)-xBaZrO3 lead-free relaxor ceramics. Ceramics International, 2020, 46, 28652-28658.	4.8	21
52	Highly sensitive methyl parathion sensor based on Au-ZrO2 nanocomposites modified graphene electrochemical transistor. Electrochimica Acta, 2020, 357, 136836.	5.2	25
53	Self-driven ultraviolet photodetectors based on ferroelectric depolarization field and interfacial potential. Sensors and Actuators A: Physical, 2020, 315, 112267.	4.1	27
54	5-Ammoniumvaleric acid stabilized mixed-dimensional perovskite submicron platelets with white light emission. Nanoscale Advances, 2020, 2, 4822-4829.	4.6	6

#	Article	IF	CITATIONS
55	Two-dimensional SnO ultrathin epitaxial films: Pulsed laser deposition growth and quantum confinement effects. Physica B: Condensed Matter, 2020, 599, 412467.	2.7	4
56	RuVO2 alloy epitaxial films: Lowered insulator–metal transition temperature and retained modulation capacity. Applied Physics Letters, 2020, 116, 192103.	3.3	8
57	High performance solar-blind UV detector based on Hf0.38Sn0.62O2 epitaxial film. Applied Physics Letters, 2020, 116, .	3.3	7
58	Study on Ca Segregation toward an Epitaxial Interface between Bismuth Ferrite and Strontium Titanate. ACS Applied Materials & Interfaces, 2020, 12, 12264-12274.	8.0	5
59	Ultrahigh Energy Efficiency and Large Discharge Energy Density in Flexible Dielectric Nanocomposites with Pb _{0.97} La _{0.02} (Zr _{0.5} Sn _{<i>x</i>} Ti _{0.5–<i>x</i>} Antiferroelectric Nanofillers, ACS Applied Materials & amp: Interfaces, 2020, 12, 12847-12856.)Ő ₃	
60	The band alignment of nonpolar m-plane ZnO1â^'xSx/Mg0.4Zn0.6O heterojunctions. AlP Advances, 2020, 10, 015314.	1.3	3
61	High-performance amorphous BeZnO-alloy-based solar-blind ultraviolet photodetectors on rigid and flexible substrates. Journal of Alloys and Compounds, 2020, 831, 154819.	5.5	12
62	Superior ferroelectric photovoltaic properties in Fe -modified (Pb,La) (Zr,Ti)O3 thin film by improving the remnant polarization and reducing the band gap. Ceramics International, 2020, 46, 15061-15065.	4.8	14
63	Effects of oxygen pressure on PLD-grown Be and Cd co-substituted ZnO alloy films for ultraviolet photodetectors. Journal of Alloys and Compounds, 2020, 833, 155032.	5.5	19
64	Citrate-driven modification of gold on titanium wire electrodes by the treatment in aqueous solutions of HAuCl4. Journal of Electroanalytical Chemistry, 2020, 872, 113991.	3.8	2
65	Ultra-wide-bandgap (ScGa)2O3 alloy thin films and related sensitive and fast responding solar-blind photodetectors. Journal of Alloys and Compounds, 2020, 834, 155036.	5.5	17
66	Electronic structure and dynamic properties of two-dimensional W Mo1â^'S2 ternary alloys from first-principles calculations. Computational Materials Science, 2020, 182, 109797.	3.0	11
67	Palladium Deposition on Nickel Microparticles by a Galvanic Replacement Reaction for Electrocatalytic Oxidation of Ethanol. ACS Applied Energy Materials, 2019, 2, 6023-6030.	5.1	8
68	Highly sensitive nitrite sensor based on AuNPs/RGO nanocomposites modified graphene electrochemical transistors. Biosensors and Bioelectronics, 2019, 146, 111751.	10.1	69
69	A gold electrode modified with a gold-graphene oxide nanocomposite for non-enzymatic sensing of glucose at near-neutral pH values. Mikrochimica Acta, 2019, 186, 722.	5.0	14
70	High energy density and efficiency in (Pb,La)(Zr,Sn,Ti)O3 antiferroelectric ceramics with high La3+ content and optimized Sn4+ content. Ceramics International, 2019, 45, 24419-24424.	4.8	26
71	Photovoltaic effect in <i>m</i> -plane orientated ZnOS epitaxial thin films. Applied Physics Letters, 2019, 115, .	3.3	8
72	Recent advances in lead-free dielectric materials for energy storage. Materials Research Bulletin, 2019, 113, 190-201.	5.2	189

#	Article	IF	CITATIONS
73	Superior energy storage performance in Pb0.97La0.02(Zr0.50 Sn0.43Ti0.07)O3 antiferroelectric ceramics. Journal of Materials Research and Technology, 2019, 8, 3291-3296.	5.8	19
74	Two-dimensional Ruddlesden-Popper perovskite nanosheets: Synthesis, optoelectronic properties and miniaturized optoelectronic devices. FlatChem, 2019, 17, 100116.	5.6	13
75	Influence of growth temperature on the characteristics of β-Ga2O3 epitaxial films and related solar-blind photodetectors. Applied Surface Science, 2019, 489, 101-109.	6.1	73
76	Mixed valence CoCuMnOx spinel nanoparticles by sacrificial template method with enhanced ORR performance. Applied Surface Science, 2019, 487, 1145-1151.	6.1	75
77	Electrochemical co-deposition synthesis of Au-ZrO2-graphene nanocomposite for a nonenzymatic methyl parathion sensor. Analytica Chimica Acta, 2019, 1072, 25-34.	5.4	70
78	Flexible dielectric nanocomposites with simultaneously large discharge energy density and high energy efficiency utilizing (Pb,La)(Zr,Sn,Ti)O ₃ antiferroelectric nanoparticles as fillers. Journal of Materials Chemistry A, 2019, 7, 13473-13482.	10.3	65
79	Superior energy-storage properties in (Pb,La)(Zr,Sn,Ti)O3 antiferroelectric ceramics with appropriate La content. Ceramics International, 2019, 45, 11375-11381.	4.8	49
80	Highâ€energy density of Pb _{0.97} La _{0.02} (Zr _{0.50} Sn _{0.45} Ti _{0.05})O _{3antiferroelectric ceramics prepared by solâ€gel method with lowâ€cost dibutyltin oxide. Journal of the American Ceramic Society, 2019, 102, 1776-1783.}	sub > 3.8	19
81	Pulsed laser deposition and characteristics of epitaxial non-polar m-plane ZnO1-xSx alloy films. Journal of Alloys and Compounds, 2019, 773, 443-448.	5.5	10
82	Structures, compositions, and optical properties of ZnCr2O4 films grown epitaxially on c-sapphire by pulsed laser deposition. Applied Surface Science, 2019, 475, 820-827.	6.1	4
83	From stannous oxide to stannic oxide epitaxial films grown by pulsed laser deposition with a metal tin target. Applied Surface Science, 2019, 466, 765-771.	6.1	8
84	Bismuth ferrite materials for solar cells: Current status and prospects. Materials Research Bulletin, 2019, 110, 39-49.	5.2	86
85	Graphene-templated synthesis of palladium nanoplates as novel electrocatalyst for direct methanol fuel cell. Applied Surface Science, 2019, 466, 385-392.	6.1	106
86	Ultraviolet polarized light emitting and detecting dual-functioning device based on nonpolar n-ZnO/i-ZnO/p-AlGaN heterojunction. Optics Letters, 2019, 44, 1944.	3.3	1
87	Theoretical investigation of the structural, electronic, and thermodynamic properties of CdS1- <i>x</i> Se <i>x</i> alloys. Journal of Applied Physics, 2018, 123, .	2.5	10
88	In situ atomic-scale observation of oxidation and decomposition processes in nanocrystalline alloys. Nature Communications, 2018, 9, 946.	12.8	14
89	Insight into the structural evolution during TiN film growth via atomic resolution TEM. Journal of Alloys and Compounds, 2018, 754, 257-267.	5.5	36
90	Anatase TiO2 single crystals with dominant {0â€ ⁻ 0â€ ⁻ 1} facets: Synthesis, shape-control mechanism and photocatalytic activity. Applied Surface Science, 2018, 444, 267-275.	6.1	42

#	Article	IF	CITATIONS
91	Electronic-structure and thermodynamic properties of ZnS1â^'Se ternary alloys from the first-principles calculations. Computational Materials Science, 2018, 149, 386-396.	3.0	12
92	Pulsed laser deposited Be x Zn 1-x O 1-y S y quaternary alloy films: structure, composition, and band gap bowing. Applied Surface Science, 2018, 433, 674-679.	6.1	10
93	Novel synthesis of core-shell Au-Pt dendritic nanoparticles supported on carbon black for enhanced methanol electro-oxidation. Applied Surface Science, 2018, 433, 840-846.	6.1	39
94	Creation of Centimeter‧ized 2 D Crystalline Film by Crystallization of Homopolymer in Solution. Chemistry - A European Journal, 2018, 24, 16440-16444.	3.3	2
95	Accounting for the thermo-stability of PdHx (xÂ=Â1–3) by density functional theory. International Journal of Hydrogen Energy, 2018, 43, 18372-18381.	7.1	12
96	Greatly enhanced photocurrent in inorganic perovskite [KNbO ₃] _{0.9} [BaNi _{0.5} Nb _{0.5} O _{3â€if}] _{0.1<!--<br-->ferroelectric thinâ€film solar cell. Journal of the American Ceramic Society, 2018, 101, 4892-4898.}	sub18	29
97	Energy storage characteristics of (Pb,La)(Zr,Sn,Ti)O3 antiferroelectric ceramics with high Sn content. Applied Physics Letters, 2018, 113, .	3.3	77
98	High electrocatalytic performance of a graphene-supported PtAu nanoalloy for methanolÂoxidation. International Journal of Hydrogen Energy, 2018, 43, 12803-12810.	7.1	37
99	Nickel Adatoms Induced Tautomeric Dehydrogenation of Thymine Molecules on Au(111). ACS Nano, 2018, 12, 9033-9039.	14.6	14
100	Exploration on the origin of enhanced piezoelectric properties in transition-metal ion doped KNN based lead-free ceramics. Ceramics International, 2018, 44, 16745-16750.	4.8	18
101	Synthesis of a 2D phosphorus material in a MOF-based 2D nano-reactor. Chemical Science, 2018, 9, 5912-5918.	7.4	14
102	Highly Flexible and Bright Electroluminescent Devices Based on Ag Nanowire Electrodes and Topâ€Emission Structure. Advanced Electronic Materials, 2017, 3, 1600535.	5.1	54
103	Pt nanoparticles modified Au dendritic nanostructures: Facile synthesis and enhanced electrocatalytic performance for methanol oxidation. International Journal of Hydrogen Energy, 2017, 42, 22100-22107.	7.1	22
104	Electroluminescence from nonpolar n-ZnO/p-AlGaN heterojunction light-emitting diode onr-sapphire. Journal Physics D: Applied Physics, 2017, 50, 115101.	2.8	5
105	Theoretical investigation on thermodynamic properties of ZnO1â^'xTexalloys. Materials Research Express, 2017, 4, 055901.	1.6	5
106	First-principles calculations of the phase equilibrium of BexZn1â^'xO alloys. Journal of Applied Physics, 2017, 121, 205101.	2.5	8
107	First-principles calculations of the thermodynamics of wurtzite and zincblende ZnO 1-x S x alloys. Physica B: Condensed Matter, 2017, 520, 1-6.	2.7	7
108	Effects of composition and temperature on energy storage properties of (Pb,La)(Zr,Sn,Ti)O3 antiferroelectric ceramics. Ceramics International, 2017, 43, 11428-11432.	4.8	86

#	Article	IF	CITATIONS
109	Magnetic order and phase diagram of magnetic alloy system: Mg <i>_x</i> Ni _{1–<i>x</i>} O alloy. Physica Status Solidi (B): Basic Research, 2017, 254, 1700085.	1.5	4
110	2D Materials: A Freeâ€Standing and Selfâ€Healable 2D Supramolecular Material Based on Hydrogen Bonding: A Nanowire Array with Subâ€2â€nm Resolution (Small 21/2017). Small, 2017, 13, .	10.0	1
111	A Freeâ€Standing and Selfâ€Healable 2D Supramolecular Material Based on Hydrogen Bonding: A Nanowire Array with Subâ€2â€nm Resolution. Small, 2017, 13, 1604077.	10.0	24
112	Coaxial‧tructured Weavable and Wearable Electroluminescent Fibers. Advanced Electronic Materials, 2017, 3, 1700401.	5.1	63
113	Generalized Selfâ€Doping Engineering towards Ultrathin and Largeâ€Sized Twoâ€Dimensional Homologous Perovskites. Angewandte Chemie - International Edition, 2017, 56, 14893-14897.	13.8	81
114	Generalized Selfâ€Doping Engineering towards Ultrathin and Largeâ€Sized Twoâ€Dimensional Homologous Perovskites. Angewandte Chemie, 2017, 129, 15089-15093.	2.0	65
115	Lead-free perovskite ferroelectric thin films with narrow direct band gap suitable for solar cell applications. Materials Research Bulletin, 2017, 95, 56-60.	5.2	23
116	SnO2 epitaxial films with varying thickness on c-sapphire: Structure evolution and optical band gap modulation. Applied Surface Science, 2017, 423, 611-618.	6.1	42
117	Good conductivity of a single component polydiacetylene film. Organic Electronics, 2017, 49, 174-178.	2.6	10
118	Enhanced photocatalytic property of BiFeO3/N-doped graphene composites and mechanism insight. Applied Surface Science, 2017, 396, 879-887.	6.1	50
119	Suppressed tanl̂´ and enhanced Qm in KCT and Ni2O3 co-modified [(K0.43Na0.57)0.94Li0.06] [(Nb0.94Sb0.06)0.95Ta0.05O3 lead-free piezoelectric ceramics. Ceramics International, 2017, 43, 2537-2540.	4.8	15
120	Strain dependent anisotropy in photoluminescence of heteroepitaxial nonpolar a-plane ZnO layers. Optical Materials Express, 2017, 7, 3944.	3.0	8
121	Raman studies of the intermediate tin-oxide phase. Physical Review Materials, 2017, 1, .	2.4	54
122	Platinum nanoparticles decorated dendrite-like gold nanostructure on glassy carbon electrodes for enhancing electrocatalysis performance to glucose oxidation. Applied Surface Science, 2016, 384, 58-64.	6.1	49
123	High recoverable energy density over a wide temperature range in Sr modified (Pb,La)(Zr,Sn,Ti)O3 antiferroelectric ceramics with an orthorhombic phase. Applied Physics Letters, 2016, 109, .	3.3	149
124	Oxygen-Driven Porous Film Formation of Single-Crystalline Ru Deposited on Au(111). Langmuir, 2016, 32, 5291-5299.	3.5	3
125	(Pb,Sm)(Zr,Sn,Ti)O ₃ Multifunctional Ceramics with Large Electricâ€Fieldâ€Induced Strain and Highâ€Energy Storage Density. Journal of the American Ceramic Society, 2016, 99, 3853-3856.	3.8	30
126	Highâ€Performance Smallâ€Amount Fe ₂ O ₃ â€Doped (K,Na)NbO ₃ â€Based Leadâ€Free Piezoceramics with Irregular Phase Evolution. Journal of the American Ceramic Society, 2016, 99, 2341-2346.	3.8	38

#	Article	IF	CITATIONS
127	Hierarchical film formation and structural characterization using MeV-ion beams. Surface and Coatings Technology, 2016, 306, 97-100.	4.8	1
128	Bottom-Up Synthesis of Metalated Carbyne. Journal of the American Chemical Society, 2016, 138, 1106-1109.	13.7	104
129	Facile synthesis of CuInS2 nanoparticles using different alcohol amines as solvent. Chemical Physics Letters, 2016, 647, 51-54.	2.6	11
130	Effects of crystallite structure and interface band alignment on the photocatalytic property of bismuth ferrite/ (N-doped) graphene composites. Journal of Alloys and Compounds, 2016, 672, 497-504.	5.5	31
131	First-principles study on thermodynamic properties of CdxZn1-xO alloys. Wuli Xuebao/Acta Physica Sinica, 2016, 65, 157303.	0.5	1
132	Research progress of metal-insulator phase transition mechanism in VO2. Wuli Xuebao/Acta Physica Sinica, 2016, 65, 047201.	0.5	7
133	Pulse Laser Deposition Fabricating Gold Nanoclusters on a Glassy Carbon Surface for Nonenzymatic Glucose Sensing. Analytical Sciences, 2015, 31, 609-616.	1.6	6
134	Leakage current transport mechanisms of La0.67Sr0.33MnO3/BaTiO3 bilayer films grown on Nb:SrTiO3. Bulletin of Materials Science, 2015, 38, 725-729.	1.7	1
135	Single-step electrochemical deposition of high performance Au-graphene nanocomposites for nonenzymatic glucose sensing. Sensors and Actuators B: Chemical, 2015, 220, 331-339.	7.8	119
136	The S concentration dependence of lattice parameters and optical band gap of a-plane ZnOS grown epitaxially on r-plane sapphire. Journal of Alloys and Compounds, 2015, 630, 106-109.	5.5	14
137	Synthesis of highly dispersed Pt nanoclusters anchored graphene composites and their application for non-enzymatic glucose sensing. Electrochimica Acta, 2015, 157, 149-157.	5.2	118
138	Characterization of Bi2Se3:Fe epitaxial films grown by pulsed laser deposition. Thin Solid Films, 2015, 577, 119-123.	1.8	8
139	Versatile Model System for Studying Processes Ranging from Heterogeneous to Photocatalysis: Epitaxial RuO ₂ (110) on TiO ₂ (110). Journal of Physical Chemistry C, 2015, 119, 2692-2702.	3.1	24
140	Controllable synthesis of palladium nanocubes/reduced graphene oxide composites and their enhanced electrocatalytic performance. Journal of Power Sources, 2015, 280, 422-429.	7.8	25
141	Oxidation-Induced Dispersion of Gold on Ru(0001): A Scanning Tunneling Microscopy Study. Journal of Physical Chemistry C, 2015, 119, 16046-16057.	3.1	6
142	The influence of oxygen flow rate on properties of SnO2 thin films grown epitaxially on c-sapphire by chemical vapor deposition. Thin Solid Films, 2015, 594, 270-276.	1.8	15
143	Polycrystalline SnO2 films grown by chemical vapor deposition on quartz glass. Vacuum, 2015, 122, 347-352.	3.5	47
144	Single-phase quaternary MgxZn1â^'xO1â^'ySy alloy thin films grown by pulsed laser deposition. Journal of Applied Physics, 2015, 117, 065301.	2.5	8

#	Article	IF	CITATIONS
145	Structural properties and enhanced bandgap tunability of quaternary CdZnOS epitaxial films grown by pulsed laser deposition. Journal of Alloys and Compounds, 2015, 650, 748-752.	5.5	11
146	First-principles study of divalent IIA and transition IIB metals doping into Cu2O. Journal Wuhan University of Technology, Materials Science Edition, 2015, 30, 458-462.	1.0	8
147	The Development of New Nonenzymatic Glucose Biosensors Using Nanomaterials. Current Nanoscience, 2015, 11, 736-747.	1.2	4
148	Facile and Rapid Synthesis of Ultrafine PtPd Bimetallic Nanoparticles and Their High Performance toward Methanol Electrooxidation. Journal of Nanomaterials, 2014, 2014, 1-7.	2.7	10
149	Annealing and characterisation of CuInS2 thin films prepared on sapphire substrates by pulsed laser deposition. Materials Research Innovations, 2014, 18, S4-22-S4-25.	2.3	0
150	Optical properties of the nonpolar a-plane MgZnO films grown on a-GaN/r-sapphire templates by pulsed laser deposition. Optical Materials Express, 2014, 4, 2346.	3.0	7
151	Direct Electrodeposition of Gold Nanostructures onto Glassy Carbon Electrodes for Non-enzymatic Detection of Glucose. Electrochimica Acta, 2014, 132, 524-532.	5.2	124
152	Synthesis of Pt–Pd bimetallic nanoparticles anchored on graphene for highly active methanol electro-oxidation. Journal of Power Sources, 2014, 262, 279-285.	7.8	108
153	Mild solution-based method for synthesizing wurtzite CuInS2 nanoplates at low temperature. Materials Letters, 2014, 123, 169-171.	2.6	10
154	Annealing effects on CulnS2 thin films grown on glass substrates by using pulsed laser deposition. Journal of the Korean Physical Society, 2014, 64, 410-414.	0.7	6
155	Structural and optical properties of single-phase ZnO1â^'S alloy films epitaxially grown by pulsed laser deposition. Journal of Alloys and Compounds, 2014, 587, 369-373.	5.5	23
156	Structural, magnetic and nanomechanical properties in Ni-doped AlN films. Journal of Alloys and Compounds, 2014, 606, 55-60.	5.5	24
157	Gold nanoparticles directly modified glassy carbon electrode for non-enzymatic detection of glucose. Applied Surface Science, 2014, 288, 524-529.	6.1	130
158	A numerical simulation study of CuInS2 solar cells. Thin Solid Films, 2014, 550, 649-653.	1.8	38
159	Resistive switching in epitaxial BaTiO3 films grown on Nb-doped SrTiO3 by PLD. Materials Science and Engineering B: Solid-State Materials for Advanced Technology, 2014, 188, 84-88.	3.5	12
160	Leakage current analysis of La0.67Sr0.33MnO3/Nb:SrTiO3 p–n junctions. Applied Physics A: Materials Science and Processing, 2014, 116, 1885-1889.	2.3	3
161	The Effects of Ta Substitution and K/Na Ratio Variation on the Microstructure and Properties of (K,Na)NbO3-Based Lead Free Piezoelectric Ceramics. Journal of Electronic Materials, 2014, 43, 1424-1431.	2.2	13
162	Tuning the composition and optical band gap of pulsed laser deposited ZnO1â^'S alloy films by controlling the substrate temperature. Journal of Alloys and Compounds, 2014, 617, 413-417.	5.5	15

#	Article	IF	CITATIONS
163	Effects of the AlN buffer layer thickness on the properties of ZnO films grown on c-sapphire substrate by pulsed laser deposition. Journal of Alloys and Compounds, 2013, 554, 104-109.	5.5	19
164	Facile synthesis of palladium–graphene nanocomposites and their catalysis for electro-oxidation of methanol and ethanol. Electrochimica Acta, 2013, 109, 570-576.	5.2	75
165	Room temperature multiferroic properties and magnetocapacitance effect of modified ferroelectric Bi ₄ Ti ₃ O ₁₂ ceramic. Journal Physics D: Applied Physics, 2013, 46, 425001.	2.8	16
166	Pulsed laser deposition of single-phase lead-free NKLNST thin films with K- and Na-excess targets. Journal of Alloys and Compounds, 2013, 567, 97-101.	5.5	12
167	Pulsed laser deposition and characterization of epitaxial CuInS2 thin films on c-plane sapphire substrates. Journal of Alloys and Compounds, 2013, 553, 282-285.	5.5	9
168	Enhancing the properties of high-temperature BiScO3–PbTiO3 piezoceramics via Bi addition. Materials Research Bulletin, 2013, 48, 3072-3076.	5.2	13
169	Solubility limits and phase structures in epitaxial ZnOS alloy films grown by pulsed laser deposition. Journal of Alloys and Compounds, 2012, 534, 81-85.	5.5	48
170	Efficient and clean synthesis of graphene supported platinum nanoclusters and its application in direct methanol fuel cell. Electrochimica Acta, 2012, 85, 84-89.	5.2	58
171	Influence of Subsurface Defects on the Surface Reactivity of TiO ₂ : Water on Anatase (101). Journal of Physical Chemistry C, 2010, 114, 1278-1284.	3.1	206
172	Evidence for the Predominance of Subsurface Defects on Reduced Anatase <mml:math xmlns:mml="http://www.w3.org/1998/Math/MathML" display="inline"><mml:msub><mml:mi>TiO</mml:mi><mml:mn>2</mml:mn></mml:msub><mml:mo stretchy="false">(<mml:mn>101</mml:mn><mml:mo) 0="" 10="" 367="" 50="" etqq0="" overlock="" rgbt="" td="" td<="" tf="" tj=""><td>7.8 (stretchy=</td><td>232 ="false">)</td></mml:mo)></mml:mo </mml:math 	7.8 (stretchy=	232 ="false">)
173	The 2×1 reconstruction of the rutile TiO2(011) surface: A combined density functional theory, X-ray diffraction, and scanning tunneling microscopy study. Surface Science, 2009, 603, 138-144.	1.9	99
174	Local ordering and electronic signatures of submonolayer water on anatase TiO2(101). Nature Materials, 2009, 8, 585-589.	27.5	298
175	Nucleation and Growth of 1D Water Clusters on Rutile TiO ₂ (011)-2×1. Journal of Physical Chemistry C, 2009, 113, 10329-10332.	3.1	33
176	Complex Growth of NanoAu on BN Nanomeshes Supported by Ru(0001). Journal of Physical Chemistry C, 2008, 112, 8147-8152.	3.1	51
177	Oxidation of Ir(111): From Oâ^'Irâ^'O Trilayer to Bulk Oxide Formation. Journal of Physical Chemistry C, 2008, 112, 11946-11953.	3.1	77
178	MgO-Supported Rhodium Particles and Films: Size, Morphology, and Reactivity. Journal of Physical Chemistry C, 2008, 112, 9040-9044.	3.1	15
179	Surface structure of Sn-doped In ₂ O ₃ (111) thin films by STM. New Journal of Physics, 2008, 10, 125030.	2.9	64
180	Long-term stability of Ru-based protection layers in extreme ultraviolet lithography: A surface science approach. Journal of Vacuum Science & Technology B, 2007, 25, 1123.	1.3	31

#	Article	IF	CITATIONS
181	Lead-free In2O3-doped (Bi0.5Na0.5)0.93Ba0.07TiO3 ceramics synthesized by direct reaction sintering. Applied Physics Letters, 2007, 90, 182903.	3.3	41
182	Self-Assembly of a Hexagonal Boron Nitride Nanomesh on Ru(0001). Langmuir, 2007, 23, 2928-2931.	3.5	216
183	Oxidation and Reduction of Ultrathin Nanocrystalline Ru Films on Silicon:  Model System for Ru-Capped Extreme Ultraviolet Lithography Optics. Journal of Physical Chemistry C, 2007, 111, 10988-10992.	3.1	25
184	RF reactive sputter deposition and characterization of transparent CuAlO2 thin films. Physica Status Solidi C: Current Topics in Solid State Physics, 2006, 3, 2895-2898.	0.8	16
185	Ultrathin Rh films on Ru(0001): Oxidation in confinement. Journal of Chemical Physics, 2006, 124, 034706.	3.0	1
186	Irregular stacking sequence in the initial growth of ultrathin Rh films on Ru(0001). Physical Review B, 2005, 72, .	3.2	5
187	Post-growth treatment effects on properties of CuInS2thin films deposited by RF reactive sputtering. Semiconductor Science and Technology, 2005, 20, 685-692.	2.0	16
188	Structural, optical and electrical properties of transparent conducting CulnO2 thin films prepared by RF sputtering. Materials Research Society Symposia Proceedings, 2005, 865, 1471.	0.1	4
189	Ru(0001) Model Catalyst under Oxidizing and Reducing Reaction Conditions:Â In-Situ High-Pressure Surface X-ray Diffraction Study. Journal of Physical Chemistry B, 2005, 109, 21825-21830.	2.6	89
190	Quasi-epitaxial growth of thick CuInS2 films by RF reactive sputtering with a thin epilayer buffer. Thin Solid Films, 2004, 451-452, 229-232.	1.8	9
191	On the composition dependence of ZnO1â^'x S x. Physica Status Solidi C: Current Topics in Solid State Physics, 2004, 1, 694-697.	0.8	28
192	Structural properties and bandgap bowing of ZnO1â^'xSx thin films deposited by reactive sputtering. Applied Physics Letters, 2004, 85, 4929-4931.	3.3	235
193	Preparation and characterization of highly (112)-oriented CuInS2 films deposited by a one-stage RF reactive sputtering process. Thin Solid Films, 2003, 431-432, 231-236.	1.8	35
194	Influence of the preparation conditions on the properties of CuInS2 films deposited by one-stage RF reactive sputtering. Thin Solid Films, 2003, 431-432, 126-130.	1.8	19
195	Deposition of CuInS2 thin films by RF reactive sputtering with a ZnO:Al buffer layer. Journal of Physics and Chemistry of Solids, 2003, 64, 2075-2079.	4.0	8
196	Heteroepitaxial growth of CuInS2 thin films on sapphire by radio frequency reactive sputtering. Applied Physics Letters, 2003, 83, 1743-1745.	3.3	35
197	SURFACE AND STRUCTURAL CHARACTERIZATION OF CuInS2 THIN FILMS DEPOSITED BY ONE-STAGE RF REACTIVE SPUTTERING. International Journal of Modern Physics B, 2002, 16, 4380-4386.	2.0	2
198	Highly (112)-Oriented CuInS2 Thin Films Deposited by a One-Stage RF Reactive Sputtering Process. Japanese Journal of Applied Physics, 2002, 41, L484-L486.	1.5	8

#	Article	IF	CITATIONS
199	(001)-Textured Cu2S Thin Films Deposited by RF Reactive Sputtering. Japanese Journal of Applied Physics, 2002, 41, 4630-4634.	1.5	24
200	Structural and optical characterization of RF reactively sputtered CuInS2 thin films. Thin Solid Films, 2002, 403-404, 62-65.	1.8	30
201	Hall effect and surface characterization of Cu2S and CuS films deposited by RF reactive sputtering. Physica B: Condensed Matter, 2001, 308-310, 1069-1073.	2.7	73
202	Characterization of RF reactively sputtered Cu–In–S thin films. Physica B: Condensed Matter, 2001, 308-310, 1074-1077.	2.7	10
203	A standing wave type ultrasonic motor. Ferroelectrics, 1999, 232, 253-257.	0.6	2
204	Studies on a new type of PbTiO3piezoelectric ceramic materials. Ferroelectrics, 1999, 229, 261-265.	0.6	2
205	The effect of doping Sb2O3in high d33• g33PZT piezoelectric ceramics. Ferroelectrics, 1997, 195, 101-104.	0.6	2
206	Correlation and comprehensive selection of the piezoelectric ignition material parameters. Ferroelectrics, 1997, 195, 97-100.	0.6	0